crystals

MDPI

Article

Tuning the Spin States of Two Apical Iron(II) Ions in a Pentanuclear Iron(II) Cluster Helicate through the Choice of Anions

Kuan-Hui Fan, Qi Huang, Xiao-Yu Fang, Lian-Wen Zhu and Zheng Yan *

College of Biological, Chemical Sciences and Engineering, Jiaxing University, 118 Jiahang Road, Jiaxing 314001, China; fanbaby321@163.com (K.-H.F.); 15857317275@163.com (Q.H.); 18663856622@163.com (X.-Y.F.); lwzhu@mail.zjxu.edu.cn (L.-W.Z.)

* Correspondence: yzheng158@mail.zjxu.edu.cn; Tel.: +86-0573-8364-3852

Received: 29 January 2018; Accepted: 28 February 2018; Published: 3 March 2018

Abstract: Spin-crossover clusters with iron(II) high nuclearity are rare. By using 3,5-bis(pyridin-2-yl)-1,2,4-triazole (bptH) as the ligand with two bidentate chelating sites, we successfully obtained three pentanuclear iron(II) cluster helicate compounds $[\{Fe^{II}(\mu\text{-bpt})_3\}_2Fe^{II}_3(\mu_3\text{-O})][Fe^{II}_2(\mu\text{-Br})(\mu\text{-bpt})(NCS)_4(H_2O)]\cdot 2H_2O\cdot C_2H_5OH$ (**1**), $[\{Fe^{II}(\mu\text{-bpt})_3\}_2Fe^{II}_3(\mu_3\text{-O})][Fe^{II}_2(\mu\text{-bpt})_2(NCS)_4]$ (**2**), and $[\{Fe^{II}(\mu\text{- bpt})_3\}_2Fe^{II}_3(\mu_3\text{-O})]I_2\cdot 2C_2H_5OH$ (**3**). Research on single-crystal structure and magnetism has indicated that tuning the spin state of two iron(II) ions in axial direction is successfully realized by regulating the different counter anions: one apical $[Fe^{II}(bpt)_3]^-$ unit exhibits spin-crossover behavior while the other $[Fe^{II}(bpt)_3]^-$ unit remains in low spin state in **1**, both apical ions are of high spin states in **2**, and are of low spin states in **3**.

Keywords: high nuclearity; spin-crossover; high spin; low spin

1. Introduction

Spin-crossover (SCO), a spin-switching phenomenon that may exist in $3d^4-3d^7$ transition metals, has been extensively explored for potential use in data storage and display devices [1,2]. Generally speaking, when an iron(II) ion with a d^6 electronic configuration is under an octahedral coordination environment, competition of electron pairing energy, and crystal field splitting-influenced arrangement of outer electrons, the iron(II) ion can adopt a low spin state (LS) or a high spin state (HS), thus influencing its magnetic behaviors. Hence, one key to preparing SCO compounds is to select a ligand that can provide appropriate cooperativity and field strength [3–5]. However, it is difficult to design and regulate SCO phenomenon at a molecular level as the coordination environment of the metal ions in compounds and any tiny structural change will probably result in the radical disappearance of the whole compound's SCO behavior because the influence of the spin transition nature on un-coordinated solvent molecules [6–9], counterions [10–12], and polymorphisms [13–15] is quite sensitive. Hence, up to now, it is still very difficult to realize directed regulation of an iron(II) ion's spin state and to carry out more in-depth studies of the relationship between magnetism and structure so as to understand and regulate the influence of the supermolecular effect on SCO behavior.

So far, among the reported SCO compounds, most are mononuclear SCO compounds. From the concept of molecular design, taking the mononuclear spin transition compounds as structural units and fiber-bridging them as one molecule through covalent bonds can produce a multi-nuclear spin transition compound. By adjusting the local coordination environment of the multi-nuclear compound, we can optimize its magnetic behavior and in this way, the magnetic behavior of the step-by-step conversion of multi-nuclear metal ions can be realized. In addition, in a multi-nuclear compound system, we can probably capture a phenomenon combining SCO behavior and magnetic exchange;

the latter may be good for enhancing the signals [16] of spin and obtaining spin transition materials with more prominent performance, helping us to understand spintronics. However, restricted by compounding means, there are few reports in this field [17–21].

In this paper, guided by the supermolecular self-assembly principle, we selected a bptH ligand with two bidentate chelating sites, mainly because this ligand should also provide an appropriate ligand field favoring the occurrence of SCO [4,22–26]; according to past literature, this kind of ligand could probably construct a multi-nucleus iron(II) ion ligand [27], and this accorded with our design concept of combining the spin-crossover nature and magnetic exchange to study spintronics. We used the self-assembly of this ligand with iron(II) ions with an octahedral coordination habit to obtain three Fe_5 cationic clusters $[\{Fe^{II}(\mu\text{-bpt})_3\}_2Fe^{II}{}_3(\mu_3\text{-O})]^{2+}$. $\{Fe_5\}$ presented a trigonal bipyramid model whereby two iron(II) ions in axial direction were of $[Fe^{II}N_6]$ configuration, and they were potential spin-crossover sites. As early as 2006 [28], Kaizaki et al. reported on a pentanuclear iron cation cluster compound $[\{Fe^{II}(\mu\text{-L})_3\}_2Fe^{II}{}_3(\mu_3\text{-O})]^{2+}$ where L was 3,5-bis (2-pyridyl) pyrazole, and the two iron(II) ions in the axial direction presented the LS state. Afterwards, similar structures—$\{Zn_5\}$ [29], $\{Ni_5\}$ [30,31], $\{Cu_5\}$ [32], $\{Mn_5\}$ [33], and $\{Fe_5\}$ [34]—were reported in succession. In 2010 [35], our research group successfully realized regulation of the spin state of two iron(II) ions in axial direction by regulating different counter anions: namely, when the anion was $[Fe^{III}{}_2(\mu\text{-O})Cl_6]^{2-}$, two iron(II) ions in axial direction presented the HS arrangement mode; when the anion was NCS^-, $ClO_4{}^-$, or I^-, two iron(II) ions in axial direction presented the LS arrangement mode. In 2016, we reported the first SCO cluster helicate $[\{Fe^{II}(\mu\text{-bpt})_3\}_2Fe^{II}{}_3(\mu_3\text{-O})][Fe^{II}{}_2(\mu\text{-Cl})(\mu\text{-bpt})(NCS)_4(H_2O)]\cdot 2H_2O\cdot C_2H_5OH$ [36], in which one apical $[Fe^{II}(bpt)_3]^-$ unit exhibited SCO behavior while the other $[Fe^{II}(bpt)_3]^-$ unit remained in the LS state. According to experience mentioned previously, we tried to seek the force that could change the mutual acting force between the $\{Fe_5\}$ molecules. After multiple attempts, we successfully obtained compounds $[\{Fe^{II}(\mu\text{-bpt})_3\}_2Fe^{II}{}_3(\mu_3\text{-O})][Fe^{II}{}_2(\mu\text{-Br})(\mu\text{-bpt})(NCS)_4(H_2O)]\cdot 2H_2O\cdot C_2H_5OH$ (**1**), $[\{Fe^{II}(\mu\text{-bpt})_3\}_2Fe^{II}{}_3(\mu_3\text{-O})][Fe^{II}{}_2(\mu\text{-bpt})_2(NCS)_4]$ (**2**), and $[\{Fe^{II}(\mu\text{-bpt})_3\}_2Fe^{II}{}_3(\mu_3\text{-O})]I_2\cdot 2C_2H_5OH$ (**3**). A study on their structure and magnetism indicated that compound **1** was the one presenting SCO behavior among $\{Fe_5\}$. Although there have been many reports on SCO compounds, we have rarely seen a structure with mixed spin states and multi-nucleus bivalent iron cluster compounds under a coordinating effect of spin transition and magnetism.

2. Materials and Methods

2.1. Reagents and Instruments

All reagents and solvents were commercial and used without further purification. FT-IR spectroscopy was performed on a Bio-Rad FTS-7 spectrometer at room temperature in the range of 4000–400 cm^{-1}. Electrospray ionization mass spectrometry (ESI-MS) in methanol was carried out on a Thermo-Finniga LCQ DeCA XP quadrupole ion-trap mass spectrometer with an electrospray ionization source. Data were analyzed by the spectrometer software MassLynx NT (version 3.4). Elemental analysis was measured with an Elementar Vario-EL CHN elemental analyzer. The kinds and amounts of solvents were determined under N_2 atmosphere with a heating rate of 10 K min^{-1} by Thermogravimetric Mass Spectrometer, STA449 F3 Jupiter-QMS 403C aedo.

2.2. Single-Crystal X-ray Diffraction

Single-crystal X-ray diffraction data of compounds **1**–**3** were collected with Mo-Kα ray (λ = 0.71073 Å) on an R-AXIS SPIDER IP diffractometer produced by Rigaku. Compound **1** was measured first at 150 K and then the temperature was rapidly increased to 298 K while continuously measuring; compound **2** was measured at 298 K; compound **3** was measured at 298 K. All data went through absorption correction. SHELXTL [37] program was used to conduct an analysis of the initial structure model with a direct method; least square method was used to refine the structure; and non-hydrogen

atom coordinates were determined through the difference value Fourier method. Displacement parameters of all non-hydrogen atoms in the compound went through anisotropic fine trimming. Hydrogen atoms were located at ideal geometric positions; therefore, they did not participate in fine trimming. Some unordered guest molecules were removed with the SQUEEZE [38] method during fine trimming. CCDC: 999096(**1**–150 K), 999097(**1**–298 K), 1495033 (**2**–298 K), 1495034 (**3**–298 K) contain the supplementary crystallographic data for this paper. These data can be obtained free of charge from The Cambridge Crystallographic Data Center at http://www.ccdc.cam.ac.uk/data_request/cif.

2.3. Magnetic Measurement

Temperature-changing molar susceptibility of the compounds was measured by a Quantum Design MPMS-XL7 SQUID instrument (Quantum Design, Inc., San Diego, CA, USA) under RSO pattern. Compound **1** was measured within the temperature range of 300–2 K. Test samples were wrapped in preservative film and diamagnetic correction was obtained with Pascal constant. The very low yield of **2** and **3** prevented the collection of reliable magnetic data.

2.4. Synthetic Procedures and Analyses

2.4.1. [{Fe^{II}(μ-bpt)$_3$}$_2$$Fe^{II}_3$($\mu_3$-O)][$Fe^{II}_2$($\mu$-Br)($\mu$-bpt)(NCS)$_4$($H_2O$)]·2$H_2O$·$C_2H_5OH$ (**1**):

We sealed the mixture of $FeBr_2$·4H_2O (0.022 g, 0.1 mmol), bptH (0.023 g, 0.1 mmol), KNCS (0.020 g, 0.2 mmol), and 10 mL ethanol solution in a 25 mL Teflon-lined reactor under 160 °C for three days and then cooled it at a velocity of 5 °C/h to room temperature; the obtained red bulk crystals were artificially purified with productivity being 52%. Elemental analysis result (%) theoretical value: C, 45.52; H, 2.89; N, 23.00; experimental value: C, 45.67; H, 2.87; N, 23.47. IR data (KBr, cm^{-1}): 3407 (m), 3070 (w), 2069 (m, NCS^-), 1604 (s), 1565 (m), 1492 (s), 1461 (s), 1409 (s), 1340 (w), 1274 (w), 1253 (s), 1151 (s), 1039 (s), 1014 (s), 898 (w), 798 (s), 746 (s), 723 (s). Mass spectrum (positive ESI; CH_3OH): m/z = 814.7 [{Fe^{II}(μ-bpt)$_3$}$_2$$Fe^{II}_3$($\mu_3$-O)]$^{2+}$.

2.4.2. [{Fe^{II}(μ-bpt)$_3$}$_2$$Fe^{II}_3$($\mu_3$-O)][$Fe^{II}_2$($\mu$-bpt)$_2(NCS)_4$] (**2**):

We sealed a mixture of $FeSO_4$·7H_2O (0.028 g, 0.1 mmol), bptH (0.029 g, 0.12 mmol), KNCS (0.033 g, 0.2 mmol), isopropanol (6 mL), and 2 mL cyclohexane in a 25 mL Teflon-lined reactor under 160 °C for three days and then cooled it at a velocity of 5 °C/h to room temperature. We obtained red tabular crystals that were then artificially purified with productivity being 15%. IR data (KBr, cm^{-1}): 3419 (s), 3070 (br, w), 2059(m, NCS^-), 1600(s), 1498(w), 1457(w), 1417(m), 1399(vs), 1261(w), 1193(w), 1020(w), 808 (w), 758(w), 728(w), 653(m), 613(m). Mass spectrum (positive ESI; CH_3OH): m/z = 814.7 [{Fe^{II}(μ-bpt)$_3$}$_2$$Fe^{II}_3$($\mu_3$-O)]$^{2+}$.

2.4.3. [{Fe^{II}(μ-bpt)$_3$}$_2$$Fe^{II}_3$($\mu_3$-O)]$I_2$·2$C_2H_5OH$ (**3**):

We sealed a mixture of FeI_2·4H_2O (0.039 g, 0.2 mmol), bptH (0.071 g, 0.3 mmol), KNCS (0.039 g, 0.4 mmol), and 10 mL ethanol solution in a 25 mL Teflon-lined reactor under 160 °C for three days and then cooled it at a velocity of 5 °C/h to room temperature. We obtained black strip crystals that were then artificially purified with productivity being 17%. IR data (KBr, cm^{-1}): 3409 (s), 3067 (w), 1605 (s), 1567 (w), 1493 (w), 1461 (w), 1417 (m), 1349 (vs), 1261 (w), 1193 (w), 1020 (w), 908 (w), 788 (w), 728 (w), 713 (m), 619 (w). Mass spectrum (positive ESI; CH_3OH): m/z = 814.7 [{Fe^{II}(μ-bpt)$_3$}$_2$$Fe^{II}_3$($\mu_3$-O)]$^{2+}$.

3. Results

3.1. Single-Crystal Structure

The structure of compound **1** was determined at 150 and 298 K, that of compound **2** was determined at 298, and that of compound **3** was determined at 298 K. For compounds **2** and **3**, the temperature change did not cause a phase change or spin transition; therefore, we only report their

structural data under room temperature. Even though **1**–**3** had different counter anions and solvent molecules, they had a similar {Fe_5} cation cluster ($[\{Fe(\mu\text{-bpt})_3\}_2Fe_3(\mu_3\text{-O})]^{2+}$) and therefore only **1** and **2** are discussed in detail.

Single-crystal X-ray diffraction measurements reveal that **1** crystallizes in the triclinic *P*-1 space group at 298 and 150 K (Table 1). At first glance, the asymmetric unit at 298 K contains one $[\{Fe^{II}(\mu\text{-bpt})_3\}_2Fe^{II}_3(\mu_3\text{-O})]^{2+}$ cation and one $[Fe^{II}_2(\mu\text{-Br})(\mu\text{-bpt})(NCS)_4(H_2O)]^{2-}$ anion and one ethanol molecule (Figure 1). The disordered water was removed by SQUEEZE [38] to achieve reasonable refinements, which were determined by thermogravimetric analysis (Figure S1) and elemental analysis [36]. The geometry of the pentanuclear cation is similar to that of our previous work [35,36] in which two terminal triple-stranded $[Fe^{II}(bpt)_3]^-$ units wrap a rare planar $[Fe^{II}_3(\mu_3\text{-O})]^{4+}$ core to form a bis(triple-helical) complex with trigonal bipyramidal topology. The rigid bis-bidentate bpt^- ligand links one apical and one equatorial Fe^{II} ion in a cis bridging mode. Six bpt^- ligands wrap around the pentanuclear cluster with offset face-to-face π-π interactions, giving rise to two homochiral $[Fe^{II}(bpt)_3]^-$ units. The apical Fe1 and Fe2 ions are located in the distorted octahedral environments with six N atoms from three bpt^- ligands. The equatorial Fe3~Fe5 ions are all in the distorted N_4O trigonal pyramidal geometries, where four N atoms come from the remaining coordination sites of two bpt^- ligands. The values of the trigonality index τ [= $(\theta_1 - \theta_2)/60$] [39,40]—where θ_1, θ_2 are defined as the two largest L–Fe–L angles in the coordination geometry—are 0.59, 0.57, and 0.68 for Fe3~Fe5 at 298 K, respectively (Table 2). Theoretically, the τ values for perfect trigonal bipyramid and square pyramid are 1 and 0, respectively [39,40]. Fe6 and Fe7 ions of the dinuclear anion have different coordination numbers and are bridged by the bpt^- ligand and a chloride ion. Fe6 ion is located in a distorted N_4Br square pyramidal environment (τ = 0.48 at 298 K) formed by one bridging chloride ion, one bpt^- ligand, and two NCS^- ligands. Meanwhile, the Fe7 ion adopts an N_4BrO octahedral geometry defined by one water and one NCS^- ligand at the axial positions; the other NCS^- ligand and the bridging bpt^- and Br^- ligands are in the equatorial plane.

Table 1. Summary of the Crystal Data and Structure Refinement Parameters for **1**, **2,** and **3**.

	1		**2**	**3**
T [K]	150	298	298	298
Chemical formula	$C_{180}H_{126}Br_2Fe_{14}N_{78}O_5S_8$	$C_{180}H_{126}Br_2Fe_{14}N_{78}O_5S_8$	$C_{100}H_{64}Fe_7N_{44}OS_4$	$C_{76}H_{60}Fe_5I_2N_{30}O_3$
Mr	4659.78	4659.78	2417.14	2417.14
crystal system	triclinic	triclinic	monoclinic	triclinic
Space group	*P*-1	*P*-1	*P*2/*c*	*P*-1
a/Å	16.859(3)	16.9483(9)	18.4797(11)	12.5313(7)
b/Å	16.949(3)	17.0488(9)	13.4662(11)	12.9876(7)
c/Å	18.934(4)	19.2261(9)	23.4082(14)	24.6635(15)
α/°	87.272(8)	88.345(2)	90	91.875(2)
β/°	79.877(7)	79.744(2)	98.471(1)	91.046(2)
γ/°	63.416(6)	64.120(1)	90	90.775(2)
V/Å^3	4760.0(16)	4910.9(4)	5761.6(7)	4010.8(4)
R_{int}	0.0775	0.0529	0.1181	0.0836
Z	1	1	2	2
μ(Mo Kα)/mm^{-1}	1.618	1.567	0.994	1.721
independent reflns	21,221	16,054	11,058	17,853
R_1 ($I > 2\sigma(I)$) [a]	0.0669	0.0618	0.0793	0.0949
wR_2 (all data) [b]	0.1822	0.1555	0.2467	0.3158
GoF	0.959	1.057	1.128	1.015

[a] $R_1 = \sum||F_o| - |F_c||/\sum|F_o|$, [b] $wR_2 = [\sum w(F_o^2 - F_c^2)^2/\sum w(F_o^2)^2]^{1/2}$.

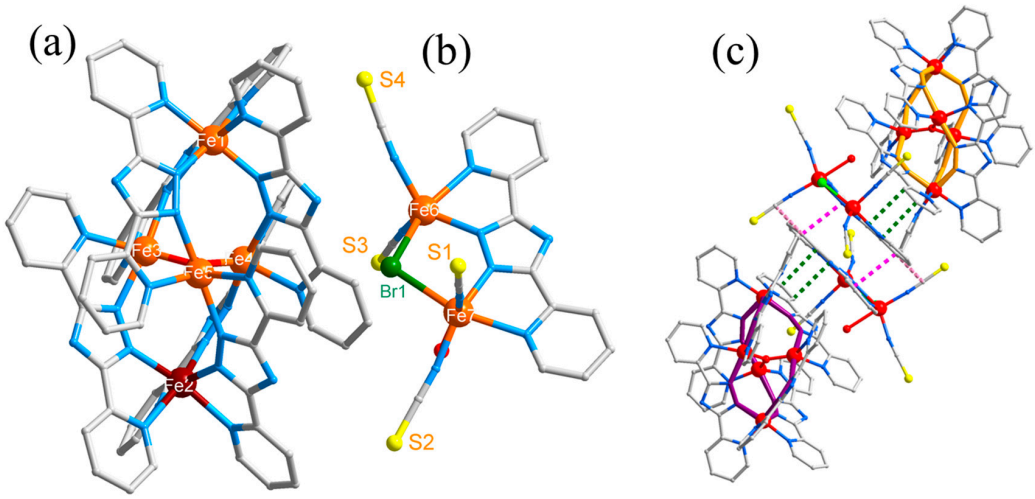

Figure 1. Structure illustrations of **1**: coordination geometries of the pentanuclear cation (**a**) and binuclear anion (**b**) and tetramer in the structure of **1** (**c**).

Table 2. The values of trigonality index τ for **1**, **2,** and **3**.

	Temperature	Fe3	Fe4	Fe5	Fe6
1	150 K	0.68	0.63	0.72	0.48
	298 K	0.59	0.57	0.69	0.48
2		Fe1	Fe3		
	298 K	0.69	0.67		
3		Fe3	Fe4	Fe5	
	298 K	0.71	0.68	0.75	

The details of the bond distance and distortion parameter around the octahedral Fe^{II} ion are effective to construct the magneto–structural relationships (Table 3) [41]. At 150 K, the average Fe1–N and Fe2–N bond distances are 1.98 and 1.99 Å, respectively, corresponding to the LS state. At 298 K, they increase to 2.00 and 2.18 Å, respectively, suggesting LS and HS states. It clearly indicates that the Fe2 ion undergoes an SCO process while Fe1 ion remains in the LS state. The values of the octahedral distortion parameter Σ, defined as the sum of absolute deviations between real and ideal values of 12 *cis* N–Fe–N angles [42], change from 59.9° to 96.6° for Fe2 ion as the temperature is increased from 150 to 298 K. Meanwhile, it displays relatively small Σ values for Fe1 ion. They are consistent with the formation of a more regular octahedron in the LS state.

Table 3. Average Bond Length (Å), Octahedral Distortion Parameter Σ (o), and Parameters of Fe-N Bond of Compounds **1–3** under Different Temperatures.

	Temperature	$Fe1–N_{av}$	Σ_{Fe1}	$Fe2–N_{av}$	Σ_{Fe2}
1	150 K	1.98	59.8	1.99	59.9
	298 K	2.00	62.0	2.18	96.6
	change	0.02	2.2	0.19	36.7
2	298 K	2.20	101.2		
3	298 K	1.98	60.5	1.98	61.4

Two dinuclear anions are linked by offset face-to-face π-π interactions between two bpt^- ligands and hydrogen bonding between bpt^- and NCS^- ligands to form an anion dimer. Meanwhile, a pair of cationic enantiomers that have opposite chirality is present on either side of the anion dimer to form

a racemic tetramer unit (Figure 1c and Figure S2). The pentanuclear cation links one anion through hydrogen bonding and offsets face-to-face π-π interactions between two bpt^- ligands, and the other anion through hydrogen bonding contact (Table S1). The tetramer units are further packed into a three-dimensional racemic supramolecular structure through intermolecular hydrogen bonding and π-π interactions (Figure S3) [36].

The single-crystal structure of compound **2** was determined at 298 K. **2** was crystallized in monoclinic space group *P*2/c. **2** contains $[\{Fe(\mu\text{-bpt})_3\}_2Fe_3(\mu_3\text{-O})]^{2+}$ cations and one $[Fe^{II}_2(\mu\text{-bpt})_2(NCS)_4]^{2-}$ anion. The disordered solvated molecules at 298 K were removed by SQUEEZE [37] to achieve reasonable refinements. The structure of the cation and anion clusters are shown in Figure 2. The structure of $[\{Fe(\mu\text{-bpt})_3\}_2Fe_3(\mu_3\text{-O})]^{2+}$ is quite similar to that in compound **1**. Five iron(II) ions are wrapped by six ligands, thus forming a pentagonal bipyramid configuration, and μ_3-O further bridges three iron(II) ions in the equatorial plane and completes their trigonal bipyramid coordination geometries. However, different from **1**, the spin state of the two iron(II) ions on axial top do not change and the average bond length of the six Fe-N bonds is 2.20 Å (Table 3), which indicates that Fe^{II} is under the HS state. It is worth noting that pentanuclear cation clusters form 1D chains (as shown in Figure 3a) among the cation clusters through supermolecular acting force π-π stacking (distance is about 3.40 Å) (Table S2).

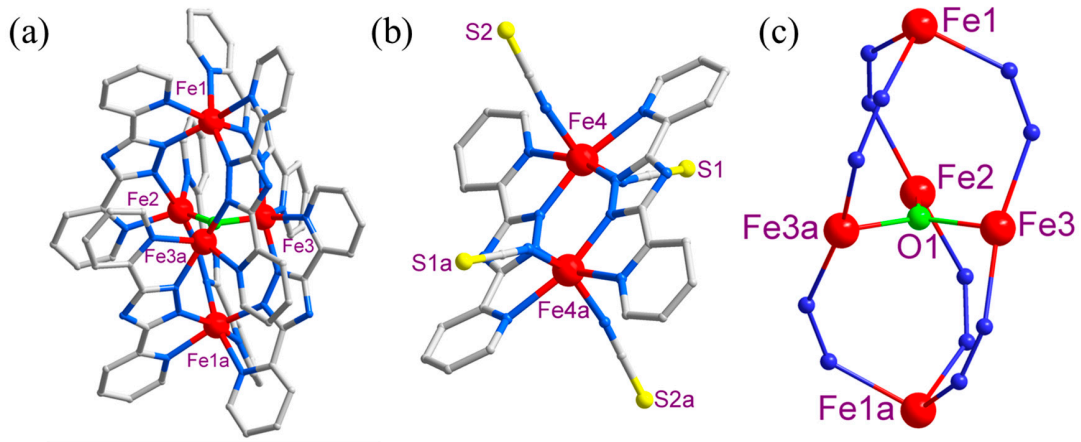

Figure 2. Structure illustrations of **2**: coordination geometries of the pentanuclear cation (**a**) and binuclear anion (**b**) and trigonal-bipyramidal core (**c**). Hydrogen atoms are omitted.

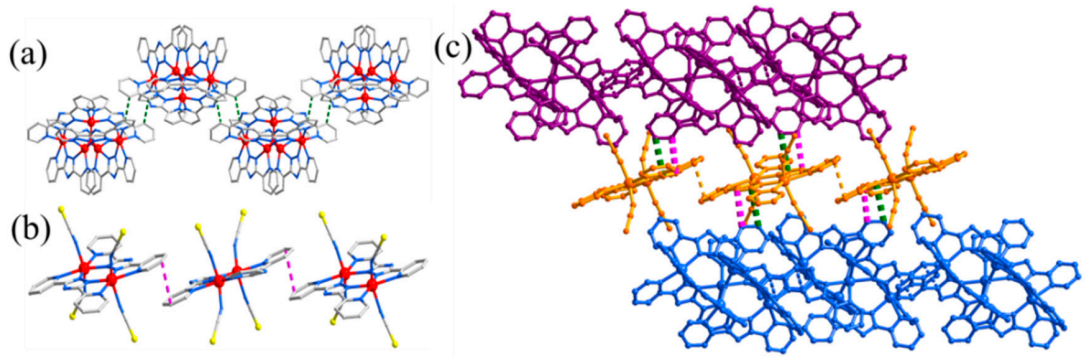

Figure 3. Structure illustrations of **2**: π-π interactions between the pentanuclear iron(II) cluster (**a**), π-π interactions between the binuclear anion (**b**), π-π interactions between the pentanuclear cation and binuclear anion (**c**).

The structure of the anion cluster is different from that in compound **1** as shown in Figure 3. The dinuclear anions have one crystallographically independent Fe4 site, which is located in the N_6

octahedral environment provided by four nitrogen atoms from two bpt^- ligands and two nitrogen atoms from two NCS^- anions (Figure 2b). Binuclear anion clusters form 1D chains among anion clusters through supermolecular acting force π-π stacking (Figure 3b) (Table S2). A supermolecular-acting force between each anion 1D chain and pentanuclear cation chain is mainly π-π stacking between a pyridine ring and a triazole ring on the ligand, thus making it extend into a 2D layer (Figure 3c).

The single-crystal structure of compound **3** was determined at 298 K. **3** was crystallized in triclinic space group *P*-1, consisting of unordered solvent water molecules among $[\{Fe^{II}(\mu\text{-bpt})_3\}_2Fe_3(\mu_3\text{-O})]^{2+}$ pentanuclear cation, I^- ion, and clusters. The structure of the cation cluster is shown in Figure 4. The structure of $[\{Fe(\mu\text{-bpt})_3\}_2Fe_3(\mu_3\text{-O})]^{2+}$ is quite similar to those in compounds **1** and **2** as shown in Figures 1a and 2a. Five iron(II) ions are wrapped by six ligands to form a pentagonal bipyramid configuration, and μ_3-O further bridges three iron(II) ions in the equatorial plane and completes their trigonal bipyramid coordination geometries. However, different from **1**, the spin states of the two iron(II) ions on axial top do not change, and the average bond length of the six Fe-N bonds is 1.98 Å (Table S3), which indicates that the iron(II) ions are under an LS state.

The structure of the anion is different from that in compounds **1** and **2** as shown in Figure S4. The anions have two crystallographically independent I^- anions; I1 ion forms three pairs of hydrogen bonds through two ethanol molecules and one pyridine from one bpt^- ligand, while the I2 ion forms four pairs hydrogen bonds through four pyridines from four bpt^- ligands. There is no obvious π-π stacking in **3**.

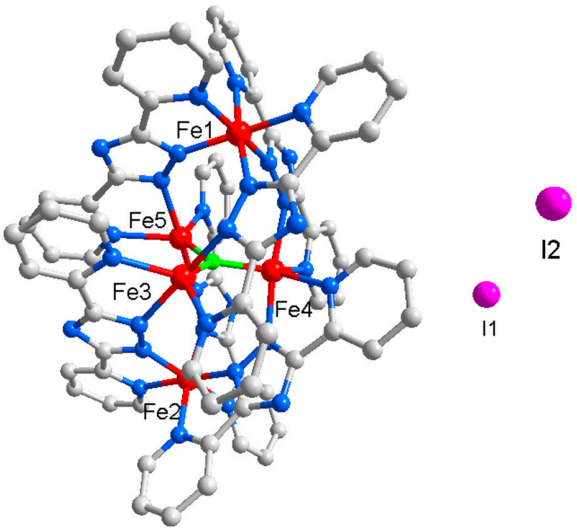

Figure 4. Structure illustrations of **3**: coordination geometries of the pentanuclear cation and I^- anion. Hydrogen atoms are omitted.

3.2. Magnetism Study

To investigate the presence of spin-crossover in compound **1**, variable-temperature magnetic susceptibility data were collected in the temperature range of 300–2 K on crystalline samples (Figure 5). The $\chi_M T$ value is 15.77 cm^3 K mol^{-1} at 300 K, which is smaller than the value (18 cm^3 K mol^{-1}) expected for six free HS ions and one LS Fe^{II} ion. On the whole, the $\chi_M T$ value smoothly decreases upon cooling with two little bulges around 210 and 70 K, and then descends more steeply to 0.76 cm^3 K mol^{-1} at 2 K, suggesting obvious antiferromagnetic coupling. Such magnetic behavior is repeatable in the subsequent heating mode (Figure S5). As mentioned above, *X*-ray crystal structure analyses clearly indicate that only Fe2 ions undergo the SCO process. To make this SCO behavior apparent, the $\chi_M T$ contributions of $[Fe^{II}{}_3(\mu_3\text{-O})]^{4+}$ core and dinuclear anion can be subtracted by the following two steps. First, the experimental $\chi_M T$ value of $[Fe^{II}{}_3(\mu_3\text{-O})]^{4+}$ core can be obtained from a similar cluster $[\{Fe^{II}(\mu\text{-bpt})_3\}^2Fe^{II}{}_3(\mu_3\text{-O})](NCS)_2{\cdot}10H_2O$, in which two apical Fe^{II} ions are in the LS state [35].

Second, after the above subtraction, the magnetic susceptibility plot between 35 K and 100 K (Fe1 and Fe2 are in the LS state) can be fitted by a simple dinuclear $S = 2$ model [43]. The fitted curve is then extrapolated to the whole temperature region to obtain the contribution of the dinuclear anion. Since the intramolecular magnetic coupling between the SCO-active Fe2 ion and central $[Fe^{II}_3(\mu_3\text{-O})]^{4+}$ core and intermolecular magnetic interactions between anions and cations are very weak [35], they can be omitted for simplification. Moreover, the Fe1 ion remains in an LS state in the whole temperature region. Thus, the magnetic susceptibility data of only Fe2 ion is obtained and shown in Figure 6. The $\chi_M T$ value at 300 K is 4.07 cm^3 K mol^{-1}, corresponding to the HS state of the Fe2 ion. Upon cooling, it clearly shows a gradual and complete SCO behavior with a spin transition temperature $T_{1/2}$ = 198 K. As comparison examples, the bulk magnetic susceptibility of compounds **1** and the chloro-analog $[\{Fe^{II}(\mu\text{-bpt})_3\}_2Fe^{II}_3(\mu_3\text{-O})][Fe^{II}_2(\mu\text{-Cl})(\mu\text{-bpt})(NCS)_4(H_2O)]\cdot 2H_2O\cdot C_2H_5OH$ compounds were determined in the 2–300 K temperature range. The results are represented in Figure S6. A similar SCO behavior was observed at much lower temperatures (near 193 K) for the chloro-analog with an approximate decrease of 5 K. In other words, $T_{1/2}$ (Cl) < $T_{1/2}$ (Br). Similar results were reported in [44].

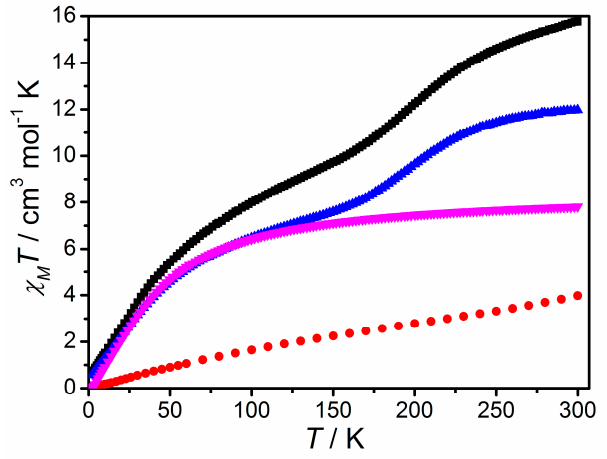

Figure 5. Plots of $\chi_M T$ vs. T for **1** (black square) and $[Fe^{II}_3(\mu_3\text{-O})]^{4+}$ core (red dots). The latter is the magnetic data of $[\{Fe^{II}(\mu\text{-bpt})_3\}_2Fe^{II}_3(\mu_3\text{-O})](NCS)_2\cdot 10H_2O$. The blue line represents the $\chi_M T$ value of **1** after subtracting the contribution of the $[Fe^{II}_3(\mu_3\text{-O})]^{4+}$ core. The blue curve between 35 K and 100 K is fitted by a dinuclear $S = 2$ model and extrapolated to 2–300 K, which represents the contribution of the dinuclear anion (pink line).

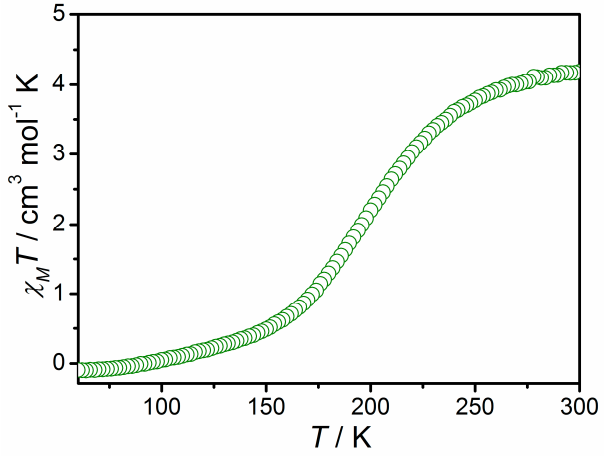

Figure 6. The $\chi_M T$ value of the Fe2 ion is obtained by subtracting the contributions of the $[Fe^{II}_3(\mu_3\text{-O})]^{4+}$ core and the dinuclear anion from **1.**

4. Discussion

The spin state of the two iron(II) ions in the axial direction was successfully realized by regulating different counter anions: one apical $[Fe^{II}(bpt)_3]^-$ unit exhibits spin-crossover behavior while the other $[Fe^{II}(bpt)_3]^-$ unit remains in a low spin state in **1.** Both apical ions are of high spin states in **2** and are of low spin states in **3**. Although these two apical iron(II) ions are coordinated by the same three bpt^- ligands, previous work has already shown that their spin states could be tuned by different counterions. Both of them are in the HS states with a $[Fe_2OCl_6]^{2-}$ anion and in the LS states with NCS^-, $ClO_4{}^-$, or I^- anions [35]. The main reason might be a variation of the supermolecular structure coordination environment of the $\{Fe_5\}$ cation cluster caused by anion replacement. Firstly, among the three compounds, hydrogen bond interactions exist between the $\{Fe_5\}$ cation cluster and the anion cluster. Different acceptor atoms of the hydrogen bonds and differences in the hydrogen bonds would probably influence the electronic configuration in the metal center, thus affecting the magnetic behavior [45,46] (see in Tables S1–S3). In addition, the π-π stacking effect between neighboring ion clusters is observed in both **1** and **2**, and the π-π effect in **2** is obviously stronger than in **1**. This effect forces the coordination sphere around the Fe(II) to accommodate this exterior constraint. Apparently, such a rearrangement would require too much energy to overcome the rigidity of the π-π stacking and is, therefore, not possible at low temperatures. In consequence, this molecular response leads to a highly distorted coordination octahedron as described above, favoring compound **2** to remain in the HS state over the whole temperature range. A similar effect was also observed recently in another iron(II) complex with the pyrene groups of the ligands and showing steadily the HS state [47]. There is no obvious π-π stacking in **3**. Similar observations have been previously reported [35]. Previous work has already shown that two apical iron(II) ions are in the LS state with I^- anions. Secondly, geometric distortion degrees that the two axial iron(II) ion coordination in the three compounds are different, which could be certified by the octahedral distortion parameter Σ (see in Table 3). For example, in compound **2**, distortion of the octahedral configuration of the two axial iron(II) ions is the most serious, which means that the electrons in the coordination atoms cannot flow into the d track of the center metal atoms very well [43], and this exerts a stabilizing effect on the HS state. The relatively large Σ values of 60.5 and 61.2 for the two apical iron(II) ions in **3** suggest that the iron(II) ions are in the LS state (Table 3). Interestingly, the SCO at the Fe2 site is associated with a more regular coordination environment about the Fe1 site, as evidenced by the increase in Σ from 59.5 to 96.6°, which also indicates that only Fe2 experiences spin transition. Similar observations have been previously reported [8,36]. Finally, a slightly shorter trans Fe2−N bond length (Table 3) should play a role in its transition, taking into account that the ligand field strength [48], Δ_0, is proportional to $1/R^6$ (Fe−N bond distances); a decrease of ca. 9.5% can be estimated for the Fe2 site with respect to the Fe1 site. These indicate that the observation of SCO in **1** relies on the presence of the Fe2 configuration providing an optimized ligand field.

5. Conclusions

In summary, by introducing an unsymmetrical binuclear anion $[Fe^{II}{}_2(\mu\text{-Br})(\mu\text{-bpt})(NCS)_4(H_2O)]^{2-}$ to the pentanuclear cluster helicate, different magnetic behaviors of two apical $[Fe^{II}(bpt)_3]^-$ units in the cationic cluster with trigonal bipyramidal topology can be obtained, in which one exhibits the SCO property while the other remains in the LS state; by introducing $[Fe^{II}{}_2(\mu\text{-bpt})_2(NCS)_4]^{2-}$ and I^- counterions to the pentanuclear $\{Fe_5\}$ cluster compounds, the spin states of two apical iron(II) ions in the cationic pentanuclear $\{Fe_5\}$ clusters can be tuned in an HS and LS state, respectively. The origin of the different spin states can ascribe to their different strengths of intermolecular interactions. Then, to our knowledge, **1** represents the second case of SCO cluster helicate, which provides an excellent example to introduce SCO properties into cluster helicates to explore multifunctional materials.

Supplementary Materials: The following are available online at www.mdpi.com/2073-4352/8/3/119/s1, Figure S1: Thermogravimetric analysis of **1**; Figure S2: Space-filling representation of the two enantiomers present in **1**;

Figure S3: Packing diagram of **1**; Figure S4. Structural illustrations of **3**: the hydrogen bond interactions. Figure S5: Plots of $\chi_M T$ vs. T for **1**; Figure S6: Plots of $\chi_M T$ vs. T for **1** and Cl-analogue. Table S1: Geometrical Parameters of the Hydrogen Bonds in Compound **1**; Table S2: Geometrical Parameters of the Hydrogen Bonds in Compound **2**; Table S3: Geometrical Parameters of the Hydrogen Bonds in Compound **3**.

Acknowledgments: This research was financially supported by the National Natural Science Foundation of China (21501067) and the Zhejiang Provincial Natural Science Foundation of China (LY18B010006).

Author Contributions: Zheng Yan conceived and designed the experiments; Kuan-Hui Fan, Qi Huang, Xiao-Yu Fang, Lian-Wen Zhu, and Zheng Yan performed the experiments; Zheng Yan wrote the paper.

Conflicts of Interest: The authors declare no conflict of interest.

References

1. Kahn, O.; Martinez, C.J. Spin-Transition Polymers: From Molecular Materials toward Memory Devices. *Science* **1998**, *279*, 44–48. [CrossRef]
2. Kumara, K.-S.; Ruben, M. Emerging trends in spin crossover (SCO) based functional materials and devices. *Coord. Chem. Rev.* **2017**, *346*, 176–205. [CrossRef]
3. Brooker, S. Spin crossover with thermal hysteresis: Practicalities and lessons learnt. *Chem. Soc. Rev.* **2015**, *44*, 2880–2892. [CrossRef] [PubMed]
4. Lochenie, C.; Schötz, K.; Panzer, F.; Kurz, H.; Maier, B.; Puchtler, F.; Agarwal, S.; Köhler, A.; Weber, B. Spin-Crossover Iron(II) Coordination Polymer with Fluorescent Properties: Correlation between Emission Properties and Spin State. *J. Am. Chem. Soc.* **2018**, *140*, 700–709. [CrossRef] [PubMed]
5. Kitchen, J.-A.; Brooker, S. Spin crossover in iron(II) complexes of 3,5-di(2-pyridyl)-1,2,4-triazoles and 3,5-di(2-pyridyl)-1,2,4-triazolates. *Coord. Chem. Rev.* **2008**, *252*, 2072–2092. [CrossRef]
6. Murphy, M.-J.; Zenere, K.-A.; Ragon, F.; Southon, P.-D.; Kepert, C.-J.; Neville, S.-M. Guest Programmable Multistep Spin Crossover in a Porous 2-D Hofmann-Type Material. *J. Am. Chem. Soc.* **2017**, *139*, 1330–1335. [CrossRef] [PubMed]
7. Liu, W.; Peng, Y.-Y.; Wu, S.-G.; Chen, Y.-C.; Hoque, M.-N.; Ni, Z.-P.; Chen, X.-M.; Tong, M.-L. Guest-Switchable Multi-Step Spin Transitions in an Amine-Functionalized Metal–Organic Framework. *Angew. Chem. Int. Ed.* **2017**, *56*, 14982–14986. [CrossRef] [PubMed]
8. Halder, G.-J.; Chapman, K.-W.; Neville, S.-M.; Moubaraki, B.; Murray, K.-S.; Létard, J.-F.; Kepert, C.-J. Elucidating the Mechanism of a Two-Step Spin Transition in a Nanoporous Metal-Organic Framework. *J. Am. Chem. Soc.* **2008**, *130*, 17552–17562. [CrossRef] [PubMed]
9. Ni, Z.-P.; Liu, J.-L.; Hoque, M.N.; Liu, W.; Li, J.-Y.; Chen, Y.-C.; Tong, M.-L. Recent advances in guest effects on spin-crossover behavior in Hofmann-type metal-organic frameworks. *Coord. Chem. Rev.* **2017**, *335*, 28–43. [CrossRef]
10. Ni, Z.-P.; Shores, M.-P. Magnetic Observation of Anion Binding in Iron Coordination Complexes: Toward Spin-Switching Chemosensors. *J. Am. Chem. Soc.* **2009**, *131*, 32–33. [CrossRef] [PubMed]
11. Ni, Z.-P.; Shores, M.-P. Supramolecular Effects on Anion-Dependent Spin-State Switching Properties in Heteroleptic Iron(II) Complexes. *Inorg. Chem.* **2010**, *49*, 10727–10735. [CrossRef] [PubMed]
12. Zhao, X.-H.; Zhang, S.-L.; Shao, D.; Wang, X.-Y. Spin Crossover in $[Fe(2\text{-Picolylamine})_3]^{2+}$ Adjusted by Organosulfonate Anions. *Inorg. Chem.* **2015**, *54*, 7857–7867. [CrossRef] [PubMed]
13. Lennartson, A.; Bond, A.-D.; Piligkos, S.; McKenzie, C.-J. Four-Site Cooperative Spin Crossover in a Mononuclear Fe^{II} Complex. *Angew. Chem. Int. Ed.* **2012**, *51*, 11049–11052. [CrossRef] [PubMed]
14. Yan, Z.; Ni, Z.-P.; Guo, F.-S.; Li, J.-Y.; Chen, Y.-C.; Liu, J.-L.; Lin, W.-Q.; Aravena, D.; Ruiz, E.; Tong, M.-L. Spin-Crossover Behavior in Two New Supramolecular Isomers. *Inorg. Chem.* **2014**, *53*, 201–208. [CrossRef] [PubMed]
15. Tao, J.; Wei, R.-J.; Huang, R.-B.; Zheng, L.-S. Polymorphism in spin-crossover systems. *Chem. Soc. Rev.* **2012**, *41*, 703–737. [CrossRef] [PubMed]
16. Létard, J.-F.; Guionneau, P.; Goux-Capes, L. Towards Spin Crossover Applications. In *Topics in Current Chemistry, Volume 235*; Springer: Heidelberg, Germany, 2004; pp. 221–249. [CrossRef]
17. Shiga, T.; Tetsuka, T.; Sakai, K.; Sekine, Y.; Nihei, M.; Newton, G.N.; Oshio, H. Cyanide-Bridged Decanuclear Cobalt−Iron Cage. *Inorg. Chem.* **2014**, *53*, 5899–5901. [CrossRef] [PubMed]

18. Rodríguez-Jiménez, S.; Feltham, H.L.C.; Brooker, S. Non-Porous Iron(II)-Based Sensor: Crystallographic Insights into a Cycle of Colorful Guest-Induced Topotactic Transformations. *Angew. Chem. Int. Ed.* **2016**, *55*, 15067–15071. [CrossRef] [PubMed]
19. Mondal, A.; Li, Y.-L.; Chamoreau, L.-M.; Seuleiman, M.; Rechignat, L.; Bousseksou, A.; Boillot, M.-L.; Lescouëzec, R. Photo- and thermo-induced spin crossover in a cyanide-bridged $\{Mo^{V}{}_{2}Fe^{II}{}_{2}\}$ rhombus molecule. *Chem. Commun.* **2014**, *50*, 2893–2895. [CrossRef] [PubMed]
20. Chastanet, G.; Carbonera, C.; Mingotaud, C.; Létard, J.-F. Atypical photomagnetic properties in a series of binuclear iron(II) spin crossover complexes. *J. Mater. Chem.* **2004**, *14*, 3516–3523. [CrossRef]
21. Chorazy, S.; Podgajny, R.; Nakabayashi, K.; Stanek, J.; Rams, M.; Sieklucka, B.; Ohkoshi, S. Fe^{II} Spin-Crossover Phenomenon in the Pentadecanuclear $\{Fe_9[Re(CN)_8]_6\}$ Spherical Cluster. *Angew. Chem. Int. Ed.* **2015**, *54*, 5093–5097. [CrossRef] [PubMed]
22. Klingele, M.-H.; Brooker, S. The coordination chemistry of 4-substituted 3, 5-di(2-pyridyl)-4H-1,2,4-triazoles and related ligands. *Coord. Chem. Rev.* **2003**, *241*, 119–132. [CrossRef]
23. Bao, X.; Liu, J.-L.; Leng, J.-D.; Lin, Z.-J.; Tong, M.-L.; Nihei, M.; Oshio, H. Spin Crossover versus Low-Spin Behaviour Exhibited in 2D and 3D Supramolecular Isomers of $[Fe^{II}(2,4\text{-bpt})_2]$·Guest. *Chem. Eur. J.* **2010**, *16*, 7973–7978. [CrossRef] [PubMed]
24. Bao, X.; Guo, P.-H.; Liu, J.-L.; Leng, J.-D.; Tong, M.-L. Crystalline-State cis-to-trans Transformation of a Two-Dimensional Spin-Crossover System. *Chem. Eur. J.* **2011**, *17*, 2335–2339. [CrossRef] [PubMed]
25. Liu, W.; Bao, X.; Mao, L.-L.; Tucek, J.; Zboril, R.; Liu, J.-L.; Guo, F.-S.; Ni, Z.-P.; Tong, M.-L. A chiral spin crossover metal-organic framework. *Chem. Commun.* **2014**, *50*, 4059–4061. [CrossRef] [PubMed]
26. Feltham, H.L.C.; Barltrop, A.-S.; Brooker, S. Spin crossover in iron(II) complexes of 3,4,5-tri-substituted-1,2,4-triazole (Rdpt), 3,5-di-substituted-1,2,4-triazolate (dpt−), and related ligands. *Coord. Chem. Rev.* **2017**, *344*, 26–53. [CrossRef]
27. Viciano-Chumillas, M.; Tanase, S.; de Jongh, L.-J.; Reedijk, J. Coordination Versatility of Pyrazole-Based Ligands towards High-Nuclearity Transition-Metal and Rare-Earth Clusters. *Eur. J. Inorg. Chem.* **2010**, *22*, 3403–3418. [CrossRef]
28. Yoneda, K.; Adachi, K.; Nishio, K.; Yamasaki, M.; Fuyuhiro, A.; Katada, M.; Kaizaki, S.; Kawata, S. An $[Fe^{II}{}_{3}O]^{4+}$ Core Wrapped by Two $[Fe^{II}L_3]$Units. *Angew. Chem. Int. Ed.* **2006**, *45*, 5459–5461. [CrossRef] [PubMed]
29. Zhu, A.-X.; Zhang, J.-P.; Lin, Y.-Y.; Chen, X.-M. Pentanuclear and Heptanuclear Helicates by Self-Assembly of d^{10} Metal Ions and a Rigid Aromatic Bis-Bidentate Chelator. *Inorg. Chem.* **2008**, *47*, 7389–7395. [CrossRef] [PubMed]
30. Hou, J.-Z.; Li, M.; Li, Z.; Zhan, S.-Z.; Huang, X.-C.; Li, D. Supramolecular Helix-to-Helix Induction: A 3D Anionic Framework Containing Double-Helical Strands Templated by Cationic Triple-Stranded Cluster Helicates. *Angew. Chem. Int. Ed.* **2008**, *47*, 1711–1714. [CrossRef] [PubMed]
31. Feng, S.-S.; Zhu, M.-L.; Lu, L.-P.; Du, L.; Zhang, Y.-B.; Wang, T.-W. Rationally designed chiral Ni5L6 clusters with the *in situ* generated tridentate ligand. Hydrothermal synthesis, crystal structures, morphology and magnetic properties. Dalton Trans. *Dalton Trans.* **2009**, 6385–6395. [CrossRef] [PubMed]
32. Ishikawa, R.; Nakano, M.; Fuyuhiro, A.; Takeuchi, T.; Kimura, S.; Kashiwagi, T.; Hagiwara, M.; Kindo, K.; Kaizaki, S.; Kawata, S. Construction of a Novel Topological Frustrated System: A Frustrated Metal Cluster in a Helical Space. *Chem. Eur. J.* **2010**, *16*, 11139–11144. [CrossRef] [PubMed]
33. Romain, S.; Rich, J.; Sens, C.; Stoll, T.; Benet-Buchholz, J.; Llobet, A.; Rodriguez, M.; Romero, I.; Clérac, R.; Mathonière, C.; et al. Multireversible Redox Processes in Pentanuclear Bis(Triple-Helical) Manganese Complexes Featuring an Oxo-Centered triangular $\{Mn^{II}{}_{2}Mn^{III}(\mu_3\text{-O})\}^{5+}$ or $\{Mn^{II}Mn^{III}{}_{2}(\mu_3\text{-O})\}^{6+}$ Core Wrapped by Two $\{Mn^{II}{}_{2}(bpp)_3\}$. *Inorg. Chem.* **2011**, *50*, 8427–8436. [CrossRef] [PubMed]
34. Gouré, E.; Gerey, B.; Clémancey, M.; Pécaut, J.; Molton, F.; Latour, J.-M.; Blondin, G.; Collomb, M.-N. Intramolecular Electron Transfers Thwart Bistability in a Pentanuclear, Iron Complex. *Inorg. Chem.* **2016**, *55*, 9178–9186. [CrossRef] [PubMed]
35. Bao, X.; Leng, J.-D.; Meng, Z.-S.; Lin, Z.-J.; Tong, M.-L.; Nihei, M.; Oshio, H. Tuning the Spin States of Two Apical Iron(II) Ions in the Trigonal-Bipyramidal $[\{Fe^{II}(\mu\text{-bpt})_3\}_2Fe^{II}{}_{3}(\mu_3\text{-O})]^{2+}$ Cations Through the Choice of Anions. *Chem. Eur. J.* **2010**, *16*, 6169–6174. [CrossRef] [PubMed]
36. Yan, Z.; Liu, W.; Peng, Y.-Y.; Chen, Y.-C.; Li, Q.-W.; Ni, Z.-P.; Tong, M.-L. Spin-Crossover Phenomenon in a Pentanuclear Iron(II) Cluster Helicate. *Inorg. Chem.* **2016**, *55*, 4891–4896. [CrossRef] [PubMed]

37. Sheldrick, M. A short history of SHELX. *Acta Crystallogr. Sect. A Found. Crystallogr.* **2008**, *64*, 112–122. [CrossRef] [PubMed]
38. Van der Sluis, P.; Spek, A.L. BYPASS: An effective method for the refinement of crystal structures containing disordered solvent regions. *Acta Crystallogr. Sect. A Found. Crystallogr.* **1990**, *46*, 194–201. [CrossRef]
39. Addison, A.-W.; Rao, T.-N.; Reedijk, J.; van Rijn, J.; Verschoor, G.-C. Synthesis, structure, and spectroscopic properties of copper(II) compounds containing nitrogen–sulphur donor ligands; the crystal and molecular structure of aqua [1,7-bis(*N*-methylbenzimidazol-2′-yl)-2,6-dithiaheptane] copper(II) perchlorate. *J. Chem. Soc. Dalton Trans.* **1984**, 1349–1356. [CrossRef]
40. Boudalis, A.-K.; Clemente-Juan, J.-M.; Dahan, F.; Tuchagues, J.-P. New Poly-Iron(II) Complexes of N_4O Dinucleating Schiff Bases and Pseudohalides: Syntheses, Structures, and Magnetic and Mössbauer Properties. *Inorg. Chem.* **2004**, *43*, 1574–1586. [CrossRef] [PubMed]
41. Halcrow, M.-A. Structure:function relationships in molecular spin-crossover complexes. *Chem. Soc. Rev.* **2011**, *40*, 4119–4142. [CrossRef] [PubMed]
42. Guionneau, P.; Marchivie, M.; Bravic, G.; Létard, J.-F.; Chasseau, D. Co.(II) molecular complexes as a reference for the spin crossover in Fe(II) analogues. *J. Mater. Chem.* **2002**, *12*, 2546–2551. [CrossRef]
43. Kahn, O. Molecular Magnetism. Wiley-VCH: New York, NY, USA, 1993. [CrossRef]
44. Darawsheh, M.-D.; Barrios, L.A.; Roubeau, O.; Teat, S.-J.; Aromí, G. Guest-Tuned Spin Crossover in Flexible Supramolecular Assemblies Templated by a Halide (Cl^-, Br^- or I^-). *Chem. Commun.* **2017**, *53*, 569–572. [CrossRef] [PubMed]
45. Agustí, G.; Cobo, S.; Gaspar, A.-B.; Molnár, G.; Moussa, N.-O.; Szilágyi, P.-Á.; Pálfi, V.; Vieu, C.; Muñoz, M.-C.; Real, J.-A.; et al. Thermal and Light-Induced Spin Crossover Phenomena in New 3D Hofmann-Like Microporous Metalorganic Frameworks Produced As Bulk Materials and Nanopatterned Thin Films. *Chem. Mater.* **2008**, *20*, 6721–6732. [CrossRef]
46. Clemente-León, M.; Coronado, E.; Giménez-López, M.-C.; Romero, F.-M. Structural, Thermal, and Magnetic Study of Solvation Processes in Spin-Crossover $[Fe(bpp)_2][Cr(L)(ox)_2]_2 \cdot nH_2O$ Complexes. *Inorg. Chem.* **2007**, *46*, 11266–11276. [CrossRef] [PubMed]
47. González-Prieto, R.; Fleury, B.; Schramm, F.; Zoppellaro, G.; Chandrasekar, R.; Fuhr, O.; Lebedkin, S.; Kappes, M.; Ruben, M. Tuning the spin-transition properties of pyrene-decorated 2,6-bispyrazolylpyridine based Fe(II) complexes. *Dalton Trans.* **2011**, *40*, 7564–7570. [CrossRef] [PubMed]
48. Tayagaki, T.; Galet, A.; Molnr, G.; Muñoz, M.C.; Zwick, A.; Tanaka, K.; Real, J.A.; Bousseksou, A. Metal Dilution Effects on the Spin-Crossover Properties of the Three-Dimensional Coordination Polymer $Fe(pyrazine)[Pt(CN)_4]$. *J. Phys. Chem. B* **2005**, *109*, 14859–14867. [CrossRef] [PubMed]